27 February 2007 Available on CMS information server **CMS NOTE 2007/012**

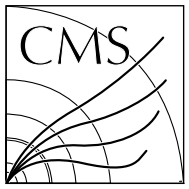

The Compact Muon Solenoid Experiment

CMS Note

Mailing address: CMS CERN, CH-1211 GENEVA 23, Switzerland

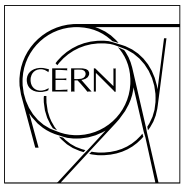

The Response of CMS Combined Calorimeters to Single Hadrons, Electrons and Muons

Nural Akchurin, Lisa Berntzon, Kazim Gümüş, Chiyoung Jeong, Heejong Kim, Sung-Won Lee, Youn Roh, Igor Volobouev, Richard Wigmans

Texas Tech University, Department of Physics, Lubbock, TX, 79409, USA

Abstract

We report on the response of the combined CMS electromagnetic (EB) and hadronic barrel (HB) calorimeters to hadrons, electrons and muons in a wide momentum range from 1 to 350 GeV/c. To our knowledge, this is the widest range of momenta in which any calorimeter system is studied. These tests, carried out at the H2 beam-line at CERN, provide a wealth of information, especially at low energies. We analyze in detail the differences in total calorimeter response to charged pions, kaons, protons and antiprotons and discuss the underlying phenomena. These data will play a crucial role in the thorough understanding of jets in CMS.

1 CMS EB and HB Calorimeters

The design and performance characteristics of the CMS EB and HB calorimeters are described in their respective technical design reports [1, 2]. The results from the first test beam of the CMS electromagnetic calorimeter are discussed in [3]. The performance of the HB was studied extensively using data from several beam tests, and those results can be found in several notes as well [4, 5, 6, 7]. We highlight only a few parameters for completeness.

EB lead tungstate ($PbWO_4$) crystals are tapered. The front-face dimensions are 2.2×2.2 cm^2 and the crystal length is 23 cm (25.8 χ_0). In order to avoid cracks in the barrel, the axes of the crystals are tilted by 3° in polar and azimuthal angles with respect to the direction of the particle track originating from the interaction point. Two avalanche photodiodes (S8148 from Hamamatsu) are glued to the back of the crystal. The *rms* noise per crystal is about 45 MeV. A minimally ionizing particle deposits about 250 MeV in the full length of the crystal [8].

The HB calorimeter is a scintillator and brass sandwich calorimeter with a segmentation of $(\Delta\eta, \Delta\phi) = (0.087, 0.087)$. The absorber consists of 40 mm thick front steel plate followed by eight 50.5 mm brass plates, six 56.5 mm additional brass plates and a 75 mm thick steel back plate. In front of the front steel plate, a 9-mm thick scintillator (Bicron BC408) is placed. The scintillators in between brass plates are 3.7 mm thick (Kuraray SCSN81). The last scintillator plate is also 9 mm thick (Bicron BC408). At $\eta = 0$, the HB calorimeter represents 5.82 interaction lengths. The HB radiation length is 1.49 cm. The scintillator plates are read out by embedded wavelength shifting fibers that transport the light to hybrid photodiodes. The *rms* noise per tower is about 150 MeV.

2 H2 Beam Line and Particle Identification

Figure 1 schematically depicts the CERN H2 beam line. The beam line is designed to operate in two distinct modes. In the high energy mode, various particles are produced when 400 GeV/c protons from the Super Proton Synchrotron (SPS) strike a production target (T2) 590.9 m upstream of the calorimeters and particle momenta range between 10 GeV/c to 350 GeV/c. In the very low energy (VLE) mode, an additional target (T22) located at 97.0 m is used for particle production and the momenta of particles are limited 1 to 9 GeV/c. As shown in Figure 1, a dog-leg configuration is utilized for the momentum selection of low momentum particles.

In the high energy mode, the T22 target and the VLE beam dump were removed from the beam line. The maximum usable beam momentum was 100 GeV/c for electrons and 350 GeV/c for hadrons. In the VLE mode, two Cherenkov counters (CK2 and CK3), two time-of-flight counters (TOF1 and TOF2) and muon counters (Muon Veto Wall, Muon Veto Front and Muon Veto Back) enabled us to positively tag electrons, charged pions and kaons, protons, antiprotons and muons.

CK2 is a 1.85-m long Cherenkov counter filled with CO_2 and was used to identify electrons in the VLE mode. At 0.7 bar, no other charged particles gave a signal and the counter was better than 99% efficient in identifying electrons. CK3 is also 1.85-m long and was filled with Freon134a [9]. The pressure in CK3 was set differently depending on the desired discrimination between electrons, pions, and kaons. For example, at lower beam momenta, ($p_b \leq 3$ GeV/c), it was set to tag electrons at 0.88 bar. Pions, kaons, and protons were uniquely identified by the time-of-flight system for this beam momenta. At higher momenta ($p_b > 4$ GeV/c), CK3 was usually run at 1.2 bar in order to separate pions from kaons and protons. Figures 2 and 3 display the identified particles in -3 and -8 GeV/c hadron beams.

Time-of-flight counters (TOF1 and TOF2) were separated by $\sim$ 55 m. Each scintillator plate measured 10×10 cm^2 in area and was 2-cm thick. Two trapezoidal shaped air-core light guides on either side of the plate funneled the scintillation light to two fast photomultiplier tubes (R5900). The analog pulses were discriminated by constant fraction discriminators and the time resolution was $\sim$300 ps. Protons were well-separated from pions (and kaons) up to 7 GeV/c with this time-of-flight system alone.

Energetic muons were tagged with Muon Veto Front (MVF) and Muon Veto Back (MVB) as well as the Muon Veto Wall (MVW) counters. MVF and MVB were large (80×80 cm^2) scintillation counters and were placed well behind the calorimeters. In order to filter out the soft muon component in the beam line, an 80-cm thick iron block was inserted in front of MVB. MVW consisted of 8 individual scintillation counters, each measuring 30×100 cm^2, placed closely behind the HB. These counters were positioned horizontally with a 2-cm overlap between them, hence covering a region of 226 cm in the vertical and 100

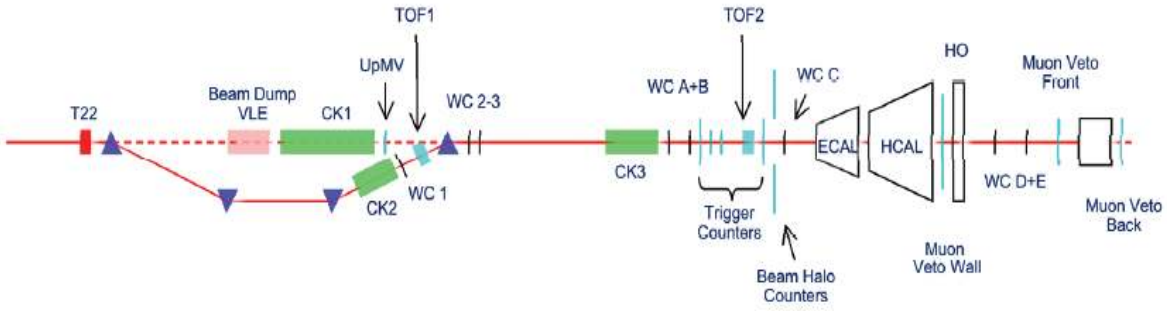

Figure 1: The CERN H2 beam line and the experimental setup are shown schematically. In the very low energy (VLE) mode, the tertiary target (T22) and a beam dump were inserted into the beam line and the low energy particles were steered through the dog-leg.

cm in the horizontal directions. In addition to tagging low momentum (2-5 GeV/c) beam muons, MVW was also used to study the details of late developing showers (see Section 3).

In addition to the afore-mentioned particle ID detectors, six delay-line chambers (WC1 through WC3 upstream and WCA through WCC downstream), four scintillation counters (S1 through S4) for triggering and four scintillation beam halo counters (BH1 through BH4) were used in the experiment. The spatial resolution afforded by the delay-line chambers was ~ 350 μm in both $x-$ and $y-$coordinates. The beam trigger typically consisted of the coincidence S1·S2·S4 which defined a 4×4 cm^2 area on the front face of the calorimeter. S4 counter was used to eliminate multi-particle events off-line since it gave a clean pulse height distribution of single and multiple particles in the beam. Four BH counters, each measuring 30×100 cm^2, were arranged such that the beam passed through a 7×7 cm^2 opening. These counters were effective in vetoing the beam halo and large-angle particles that originated from interactions in the beam line.

The particle mixture in the VLE configuration varied with beam momentum. The beam consisted of 7% pions, 0.1% kaons, and 2.1% protons at +4 GeV/c, and the remaining particles were positrons and muons. At +8 GeV/c, the beam contained 32.5% pions, 1.1% kaons and 3.3% protons, and again the remaining fraction consisted of positrons and muons. In the negatively charged beam, the particle mixture was approximately the same but the antiproton fraction was much reduced compared to that of proton's in the positive beam. In order to enrich the hadron content of beam triggers at low energies, we often elected to run with a S1·S2·S4·$\overline{\text{MVB}}$ trigger.

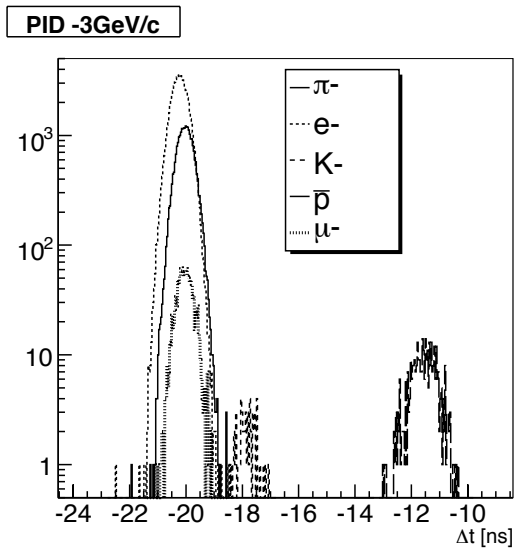

Figure 2: The particle identification was carried out with two Cherenkov counters (CK2 and CK3), two time-of-flight counters (TOF1 and TOF2), and muon veto wall counters (MVB) in the VLE mode. The -3 GeV/c beam data is shown as an example.

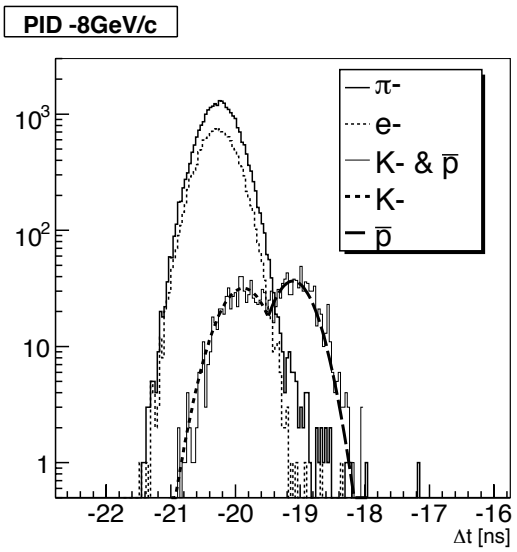

Figure 3: The same as Figure 2 but for a -8 GeV/c hadron beam (see text for details).

3 Response of the Combined Calorimeter System

The e/h ratio of a calorimeter is a measure of its response to particles developing electromagnetic showers compared to particles developing non-electromagnetic ones. The e/h ratio for the CMS electromagnetic calorimeter based on fully sampling $PbWO_4$ crystal is ~ 2.6. The hadronic calorimeter, which is a sampling device with alternating brass and scintillator plates, has an e/h ratio of ~ 1.4 [7]. Because of this large difference between the e/h values of the EB and HB, the combined CMS calorimeter system poses interesting challenges.

Both the EB and HB calibrations were carried out with 50 GeV/c electrons. The HB calibration was performed before the EB supermodule was mounted in front of the HB, and the electron beam was directed at the center of each tower. Similarly, the EB calibration data were collected by pointing the beam to a selected set of crystals that formed a tight grid pattern. There are several different algorithms in CMS to calibrate the EB crystals. We studied these algorithms carefully and found that although there are differences between these methods, the conclusions we draw in this paper are largely insensitive to them. Because we calibrated the EB and HB compartments with the same particles (electrons and positrons), the reconstructed energy is simply the sum of energies recorded by the EB and HB. The combined response of the system is then the ratio between the reconstructed energy and the available energy deduced from the beam momentum. The calibration strategy adopted here sets the energy scale of each compartment in exactly the same way. Alternative methods exist, see for example [10].

As an example, the response functions for 5 and 100 GeV/c π^- beam are displayed in Figure 4 for the EB, HB and the sum of signals which also includes the correction for a small energy leakage from the back of the calorimeter. The EB signal is constructed by adding the calibrated signals from 7×7 crystals, and for the HB, 3×3 towers are summed. The energy leakage, which becomes more important at high energies, is calculated from MVW signals (see Figure 8). As Figure 4 clearly shows, a sizable fraction of pions interact in the EB as evidenced by the second peak in Figure 4 a) and d). The non-interacting pions deposit little energy in the EB (the first peak). The signal distributions from the HB complementarily illustrate the late (the second peak Figure 4 b) and e)) and the early (the first peak) developing showers.

If we had elected to calibrate the EB compartment with electrons and the HB with penetrating pions, the total calorimeter response would be systematically larger compared to what is shown in Figure 6. There

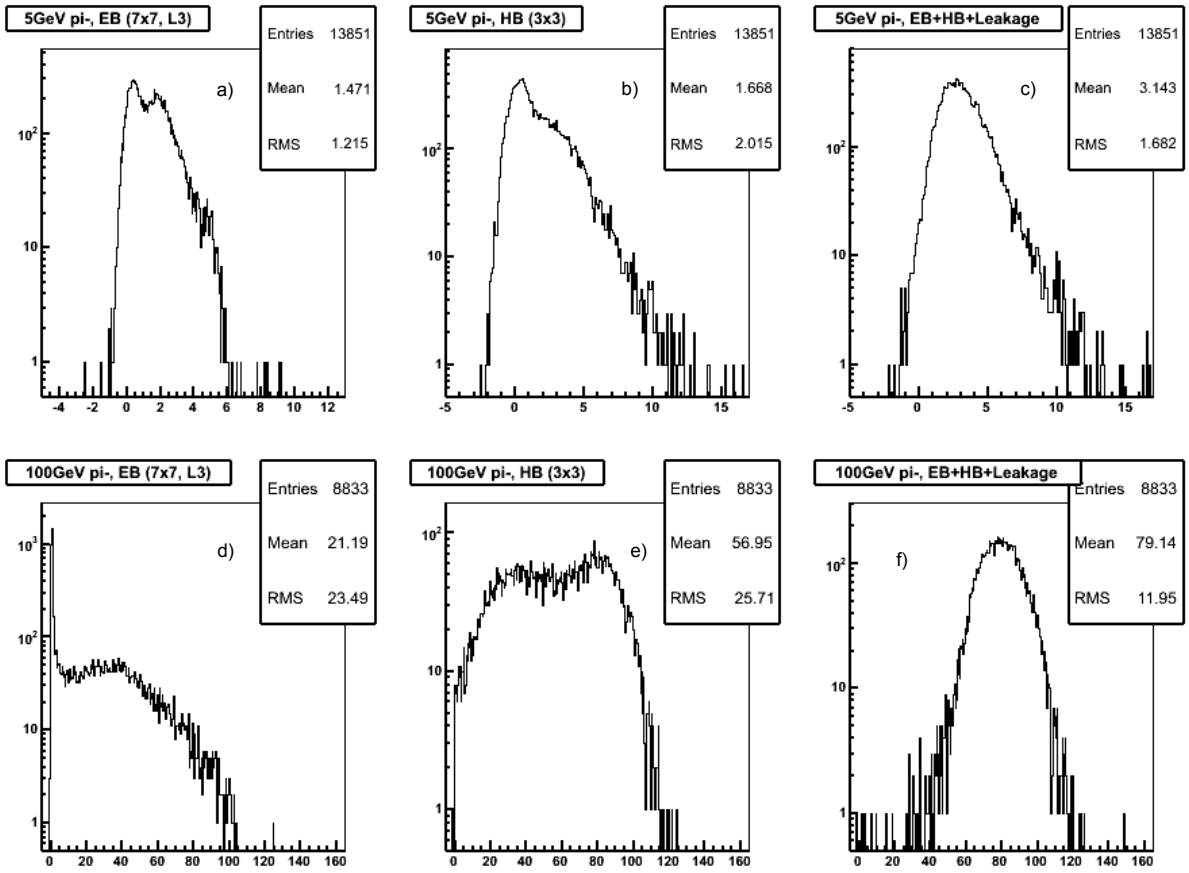

Figure 4: The response functions for 5 and 100 GeV/c negative pions are shown above for the EB (a and d), HB (b and e), and the sum of all signals from the combined system (c and f) which also includes the energy leakage from the back of the HB.

are serious consequences if we made such a choice. First, it would clearly increase the non-linearity of the entire system because the method applies larger than unity weight to the HB signals. Since high energy pions on average deposit more energy in the HB, they are more affected by this than low energy pions. Second, this approach increases the difference between the responses to early and late starting showers since these showers deposit a different fraction of their energy in the HB. It thus introduces an undesired bias in the reconstructed energy, depending on the starting point of the showers. Third, pion calibration of the HB is only correct at the pion energy at which the calibration is performed. Additional corrections for pions of other energies would be needed.

Figure 5 shows the combined response of the CMS EB+HB calorimeters to a variety of particles in a wide range of momenta ($1 \leq p_b \leq 350$ GeV/c) as a function of beam momentum. At 5 GeV/c, the antiproton response is $\sim$ 70% of the electron response. The responses to charged pions and proton are 62% and 47% of the electron response, respectively. However, at a given momentum, the available energy that is converted to a calorimeter signals is different for different particles. For pions and kaons, the available energy is their kinetic energy. For protons, it is also the kinetic energy and for antiprotons, the available energy for a calorimetric signal equals the kinetic energy plus twice the rest mass of proton. In Figure 6, the same data are plotted against the available energy. In first approximation, one would expect the same response characteristics for all hadrons when the data are represented this way. We will return to the discussion of subtle differences later in this section after reviewing the combined calorimeter response to electrons and muons.

The response of the calorimeter to electrons is linear within $\pm$2% over the full momentum range of 1 to 100 GeV/c. The very low energy data analyses are still ongoing and a careful comparison with EGS simulation must be made in order to finalize these data points. In the case of muons, the lowest energy particles (< 2 GeV/c) range out in the calorimeters. Figure 7 shows the signals observed by one MVW

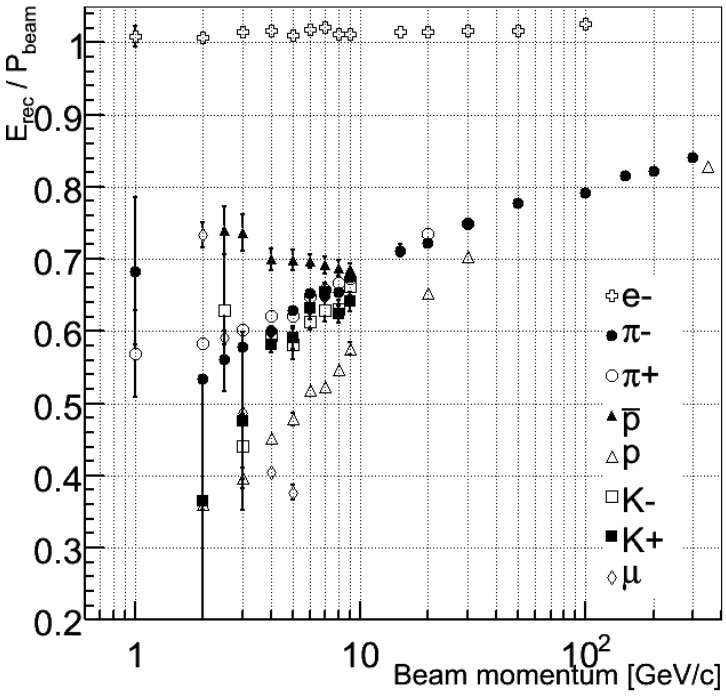

Figure 5: The response of the combined calorimeter systems to eight different particles is shown as a function of the beam momentum. Both the EB and HB are calibrated with 50 GeV/c electrons.

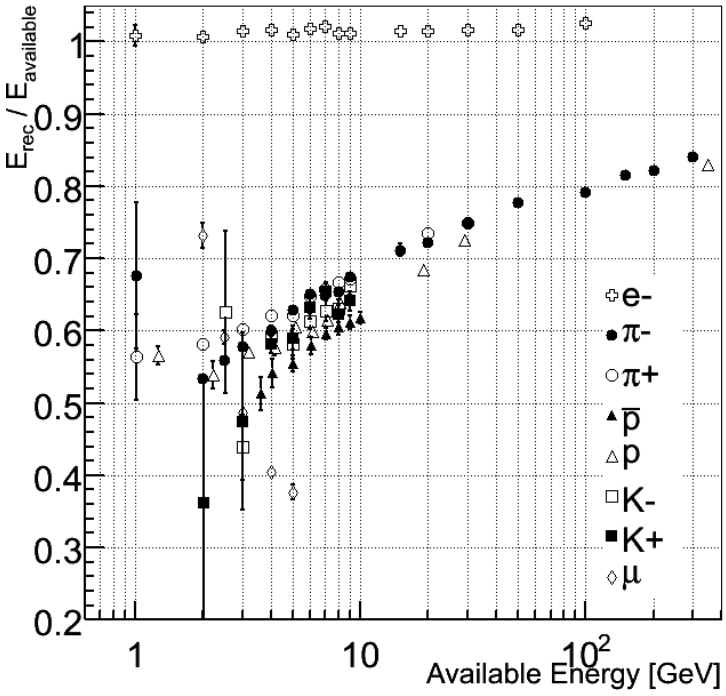

Figure 6: The same data as in Figure 5 but the calorimetry response is plotted against the available energy.

counter for four low energy pion beams. At 1 GeV/c, there is neither detectable energy leakage nor muons behind the calorimeters. At 2 GeV/c, in addition to the *mip* signal, we observe some energy leakage due mainly to neutrons exiting the back of the HB. At 9 and 50 GeV/c, leakage in the form of *mip*s and neutrons is clearly increased. At high energies, the energy leakage reaches an average level of 2−3 GeV with large event-to-event fluctuations. The measured leakage is added event-by-event to the calorimeter signal. The hadron outer (HO) calorimeter is designed to measure this leakage. In this analysis, however, we chose to use MVW instead since it afforded the largest coverage behind the HB for the beam spot analyzed here; the HO covered only half. Figure 8 shows the energy calibration of MVW.

It is interesting to note that a 2-GeV/c muon generates a considerable calorimeter response, more than 70% that of an electron as shown in Figures 5 and 6. The muon response, $E_{\rm rec}/E_{\rm available}$, quickly decreases as its momentum increases, since the deposited energy is in first approximation energy independent.

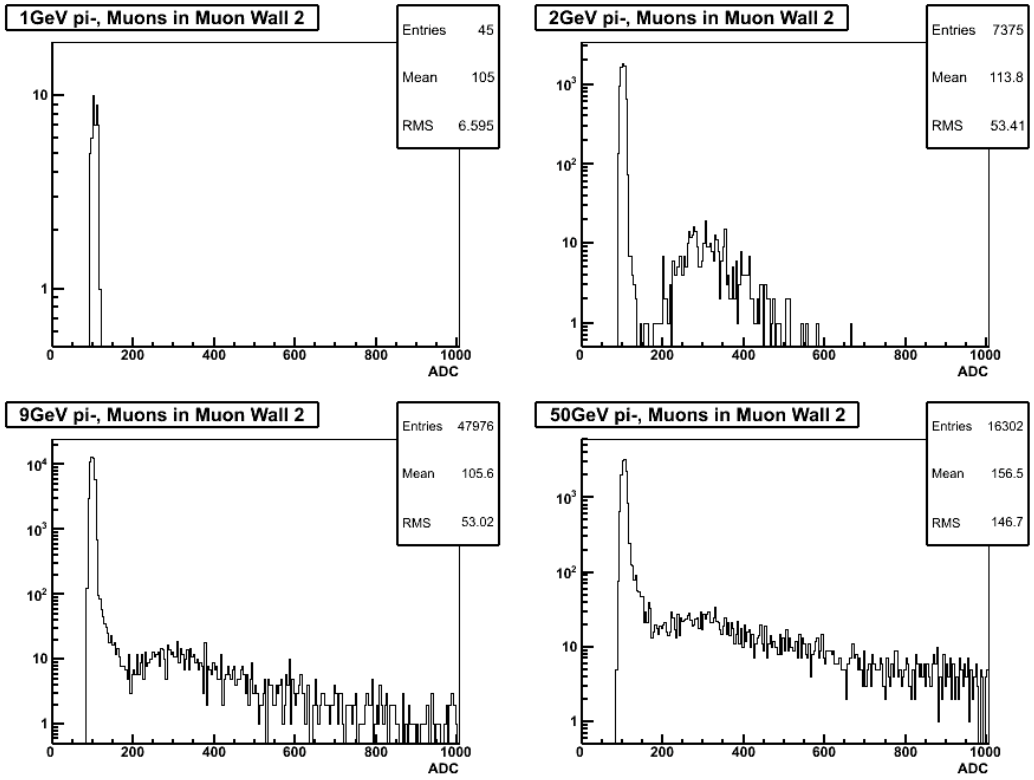

Figure 7: The signal distribution from a MVW clearly demonstrates that muons with less than 2 GeV range out in the calorimeters. As the beam energy is increased, the energy leakage also increases as evidenced by the high-side tail of the pedestal peak.

Figure 9 show the fraction of energy deposited in the EB for pions and (anti)protons. At low energies, a significant fraction of the available energy is deposited in the EB. The EB calorimeter represents a significant absorber in front of the HB ($\sim 1\lambda_{\rm int}$), and once the first interaction takes place in the EB, essentially all the π^0 component produced in that interaction of the shower is registered by it.

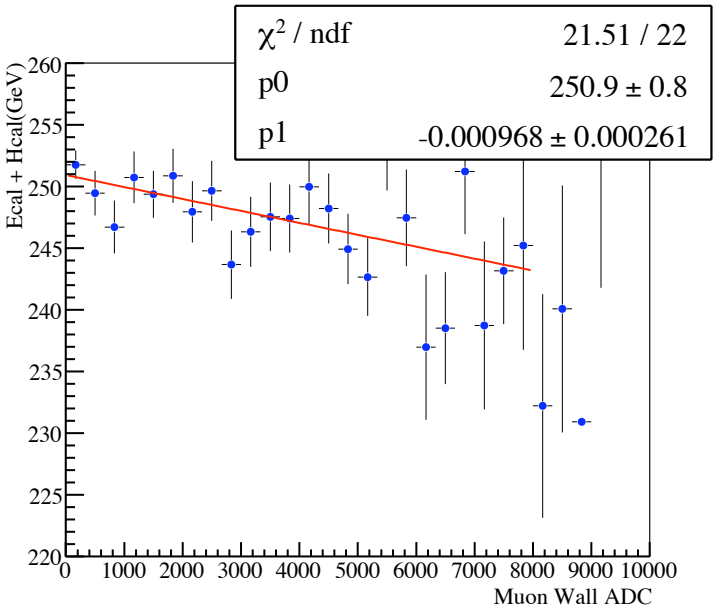

Figure 8: Three MVW counters are used to register leakage energy behind the HB (The case of 300 GeV/c pions is shown above). The three signals are summed after the gain equalization based on *mip* peaks.

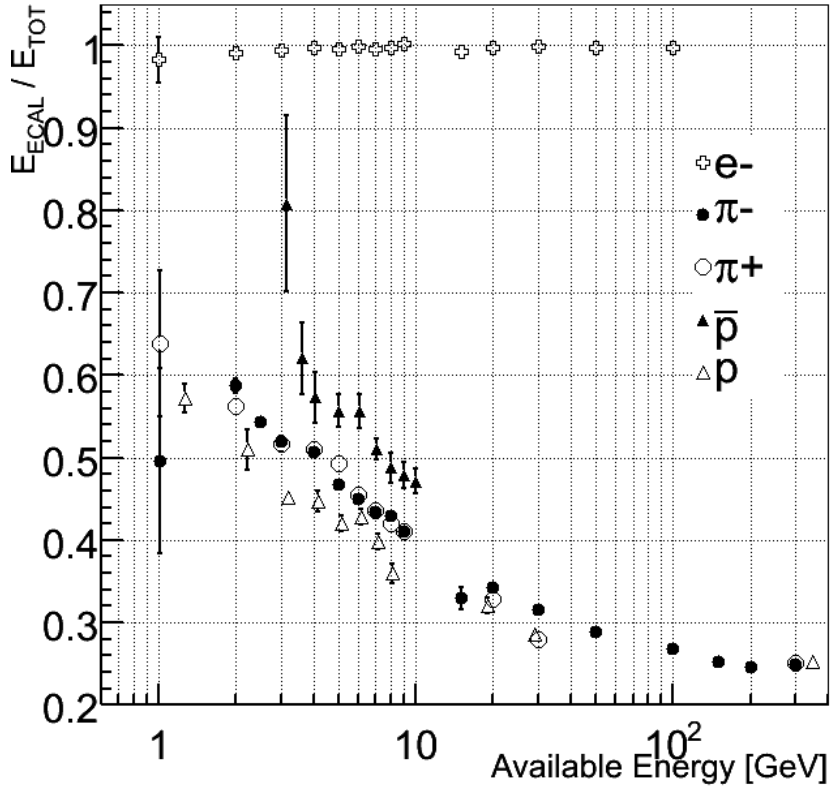

Figure 9: The fraction of energy deposited in the EB is plotted against the available energy for electrons, charged pions and (anti)protons. The total energy is the sum of energies observed by the EB, HB and the muon veto wall.

We now return to the analyses of the combined calorimeter response to hadrons in Figures 5 and 6.

- The response to π^+ is systematically larger than the π^- response, more so as the energy decreases. This can be understood from the characteristics of the charge exchange reactions, $\pi^+ + n \rightarrow \pi^0 + p$ (I) and $\pi^- + p \rightarrow \pi^0 + n$ (II). In these reactions, a large fraction of the pion energy is carried by the final-state π^0, which develops electromagnetic showers. Therefore, the calorimeter response to pions interacting this way is close to 1. Since the target material ($PbWO_4$) contains about 50% more neutrons than protons, the relative effect of reaction (I) will be larger than that of reaction (II), and therefore, the calorimeter response to π^+ should be expected to be larger than the π^- response.

- The response to protons is systematically lower than the pion response. This effect, which is also observed at high energy, is a result of the fact that π^0 production is, on average, smaller in proton induced showers. This is a consequence of the baryon number conservation requirement, which favors the production of leading baryons, while pion induced reactions may have leading π^0s. This effect was clearly observed in the HF calorimeter [11], where it caused a response difference in excess of 10%. Since the e/h values of EB+HB are smaller than for the HF, the effects are correspondingly smaller but nevertheless significant.

- Since the total cross sections for baryon induced interactions are larger than for pions, a larger fraction of the baryons will start showering in the EB. This is illustrated in Figure 10, which shows that 41% of the pions penetrate the EB without starting a shower, versus only 35% for protons. The effective thickness of the EB is thus $1.05\lambda_{\rm int}$ for protons and $0.89\lambda_{\rm int}$ for pions. Since the total cross sections for protons and antiprotons are about the same, the same holds for the effective EB thickness.

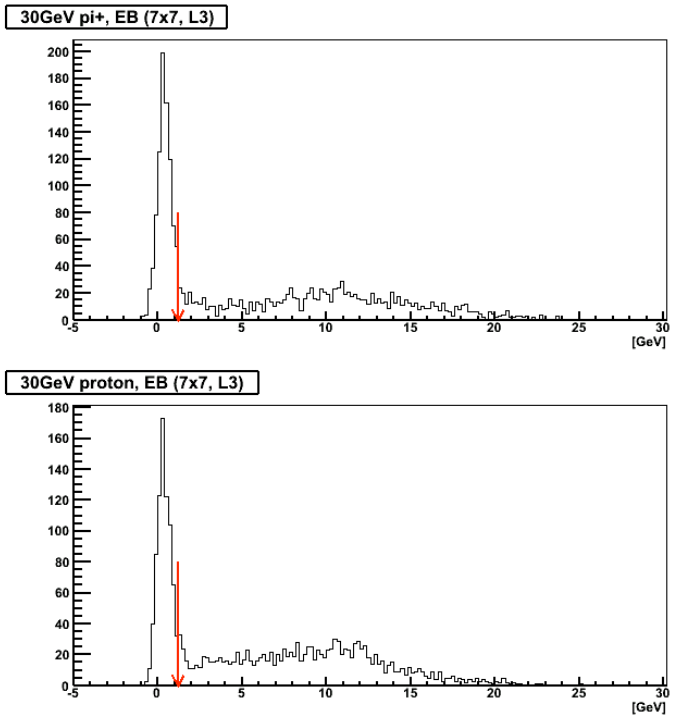

Figure 10: The signal distributions from the EB are shown for 30 GeV/c pions (top) and protons (bottom). The arrow indicates where the cut is applied (1.2 GeV) to separate the penetrating pions and protons from the interacting ones. 41% of pions are penetrating or deposit energy in the EB that is consistent with a *mip* signal. However, only 35% of protons deposit comparable energy.

- The previous two points make it possible to understand Figure 9, which shows the average energy sharing between the EB and HB for hadronic showers. The fraction of the energy recorded by the EB increases from $\sim$ 25% at the highest energies to $\sim$ 60% at 2 GeV. Remarkably, at the same

energies, protons deposit on average less than pions in the EB, while antiprotons deposit more than pions. Antiprotons start their showers, on average, earlier than pions and therefore a larger fraction of the energy ends up in the EB. At first sight, one would expect the same for proton induced showers. However, when a proton interacts in the EB, the final state should contain 2 baryons, which limits the energy available for π^0s. And since the EB, for all practical purposes, only sees the π^0 component of the showers, this effect suppresses the proton signal in the EB, despite the fact that protons are more likely to start their showers in the EB compared to pions. The requirements of baryon number conservation do not limit π^0 production for antiproton induced showers. In first approximation, there is no difference with pion induced showers. Therefore, the EB/HB energy sharing properly reflects the difference in interaction length in this case.

- The effects described above also explain why the antiproton response is systematically smaller than the pion response (Figure 5). Antiprotons are more likely to start showering in the EB compared to the pions. Pions deposit, on average a larger fraction of their energy in the HB. And since the e/h value of the HB is smaller than for the EB, the pions benefit more from the increased response to the non-em shower components.

- The effects of baryon number conservation described above have an equivalent in the case of kaon induced showers, where the requirements of strangeness conservation preclude the production of leading π^0, and therefore limit the average em shower fraction, and thus the calorimeter response, compared to pions. Our statistics are insufficient to verify these effects.

- In order to study the effects of the very different e/h values of the EB and HB, we subdivided our pion event samples into "early" and "late" starting showers. The distinction was made on the basis of the energy fraction observed in the EB. For late starting showers, this energy fraction was chosen such that events in the *mip* peak in the EB were selected. These pions thus only lost some energy by ionization in the EB and underwent the first nuclear interaction in the HB. In early starting events, the pions deposited a larger fraction of their energy in the EB. The pion response for these two classes of events is shown as a function of available energy in Figure 11, together with the overall pion response. For the lowest energies it was not possible to select a clean sample of "late" events, since the *mip* peak was not clearly resolved in the EB distribution (see Figure 4.a). Figure 11 shows an increasing discrepancy between the calorimeter responses to early and late showers as the particle energy decreases. The discrepancy itself reflects the different e/h values. Late showers deposit almost no energy in the EB, and therefore their response is completely determined by the (more compensating) HB. Early showers experience the strong (by a factor 2.6) reduction in the response to the non-em shower component deposited in the EB. The fact that the discrepancy increases at lower energy reflects the changes in the longitudinal shower profile also observed in the energy sharing plot (Figure 9). The larger the average fraction of the shower energy deposited in the EB, the larger the response discrepancy between showers that start in the EB and those that don't.

- At the lowest particle energies, the downward trend in the pion response is observed to reverse for early developing showers (see Figure 11). The minimum response is observed at 4 GeV, and at lower energies the response increases. A similar effect was observed by the ZEUS Collaboration [12], who also saw the response of their uranium/scintillator calorimeter increase for energies below 5 GeV. The explanation for this phenomenon is the fact that at lower energies, a gradually increasing fraction of the particles range out without inducing any nuclear reaction. Nuclear reactions are responsible for the "invisible energy" losses that increase e/h and thus reduce the hadronic response. The calorimeter will respond to such non-interacting particles in the same way it responds to muons, and below 2 GeV, where all such particles are completely stopped in the calorimeter, the response is equal to that of electrons in the EB and even larger than that (by a factor *mip*/e) in the HB.

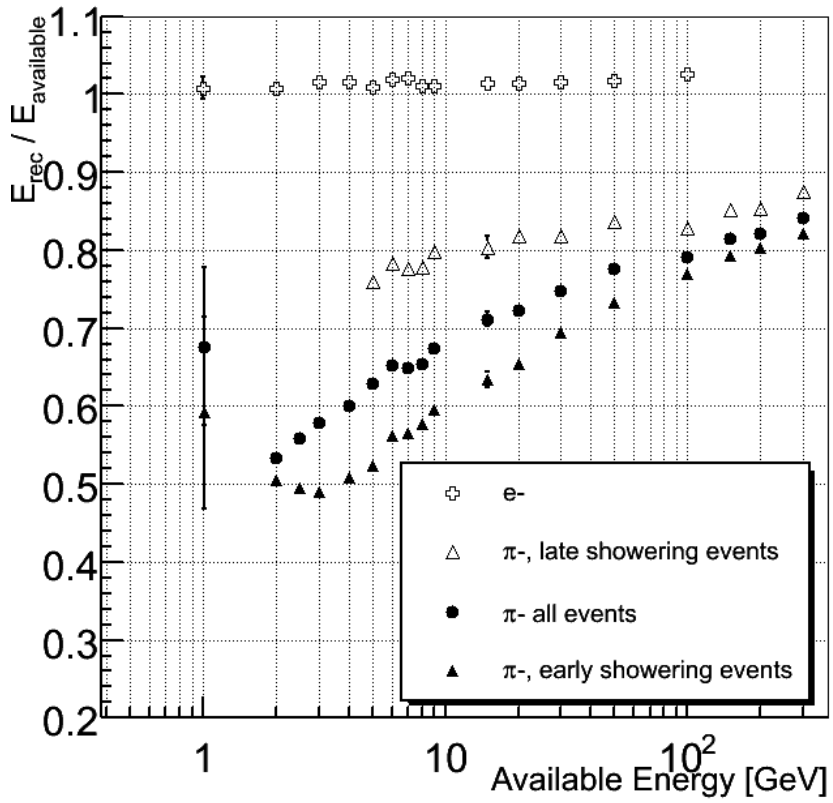

Figure 11: The response of the combined calorimeters is shown against the available energy for pions and electrons. The marked difference in response for the early and late developing showers initiated by pions is discussed in the text.

4 Raw Energy Resolution

The energy resolution of the combined CMS calorimeter system is shown in Figure 12. The black circles represent the energy resolution for all negatively charged pions. As explained in the previous section, we divide our pion sample into early and late showering categories and compute energy resolutions based on the *rms* and mean values of these distributions. Early showering events that deposit good fraction of their energy in the EB give markedly better energy resolution at low energies compared to all events. The EB calorimeter essentially acts as a π^0 detector and efficiently samples π^0s that are predominantly produced at the first interaction. As the energy increases, the difference in energy resolution between the early/late developing showers is reduced except when the leakage fluctuations for the late developing showers degrade the resolution at the highest energies. Addition of MVW signal improves the resolution at a few percent level but does not fully recover it.

The energy resolution of the combined calorimeters cannot satisfactorily be described with the conventional expression for resolution that involves the stochastic, electronic noise, and constant terms for the full energy range obtained in these tests. The complete analysis and optimization of energy resolution is on-going and will be reported.

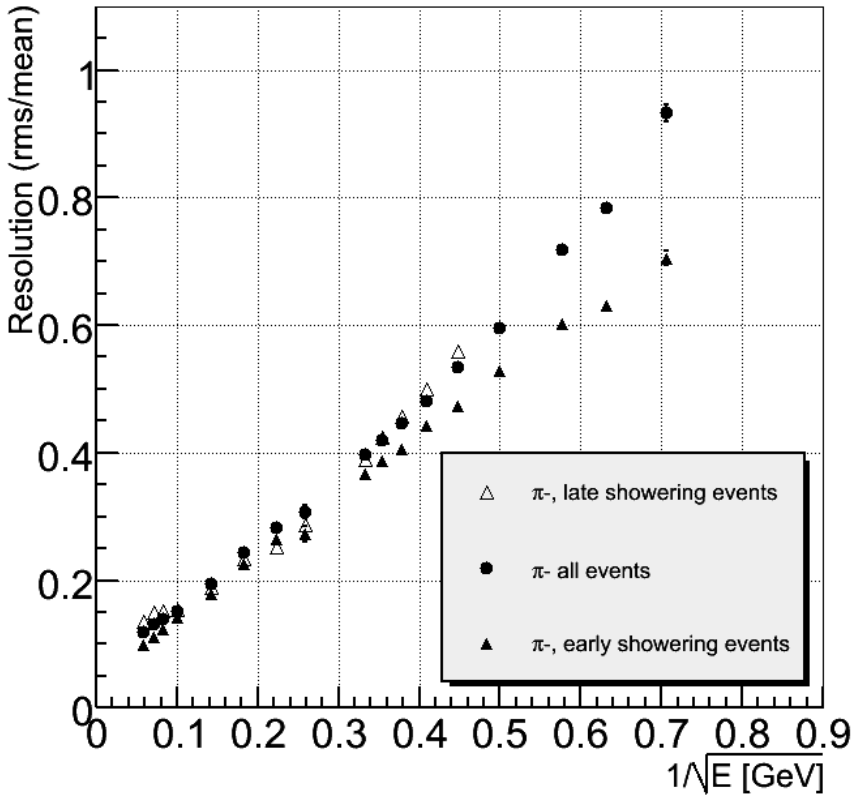

Figure 12: The energy resolution of the combined CMS calorimeters for negatively charged pions based on the test beam data in 2006 is shown above. Full circles represent data from all pions that pass the event selection criteria. The full and open triangles indicate early and late showering events in the calorimeter (see text for details).

References

[1] CMS Collaboration, The Electromagnetic Calorimeter Technical Design Report, CERN/LHCC 97-33 (1997).

[2] CMS Collaboration, *The Hadron Calorimeter Project Technical Design Report*, CERN/LHCC 97-31 (1997).

[3] P. Adzic *et al*, Eur. Phys. J. C **44**, s02, 1-10 (2006).

[4] V. Abramov *et al*, Studies of the Response of the Prototype CMS Hadron Calorimeter, Including Magnetic Field Effects, to Pion, Electron and Muon Beams CMS Note-2000/003;

[5] G. Baiatian *et al*, Energy Response and Longitudinal Shower Profiles Measured in CMS HCAL and Comparison With Geant4, CMS NOTE-2006/143.

[6] G. Baiatian *et al*, Synchronization and Timing in CMS HCAL, CMS NOTE-2006/139.

[7] G. Baiatian *et al*, Design, Performance, and Calibration of CMS Hadron-Barrel Calorimeter Wedges, CMS NOTE-2006/138.

[8] W. Bertl *et al*, Eur. Phys. J. C **41**, s02, 11-17 (2005).

[9] Freon134a is an ozone-friendly gas. Based on the measurements during the beam test, we find Freon 134a's refractive index to be 1.00065, which is also consistent with the estimates based on its molecular weight.

[10] D. Green and E. Yazgan, CMS NOTE in preparation.

[11] N. Akchurin *et al*, Nucl. Instr. and Meth. **A408** (1998) 380-396.

[12] A. Andresen *et al*, Nucl. Instr. and Meth. **A290** (1990) 95.